2021 IEEE Conference on Antenna Measurements & Applications (CAMA)
15-17 November 2021, Antibes Juan-les-Pins, France

High Resolution Spintronics Probe-Array Technology Solutions for Very Near-Field Scanning

S. Wane[$], Q.H. Tran [$], T.V. Dinh[$], F. Terki[$], D. Bajon[$], V. Huard[⊥], L. Nyssens[†], J.-P. Raskin[†], D. Lederer[†], P. Eudeline[Λ], A. Bousseksou[§]

[$]eV-Technologies, [⊥]Dolphin-Design, [†]ICTEAM-UCL, [Λ]Thales, [§]LCC-CNRS

2021 IEEE Conference on Antenna Measurements & Applications (CAMA) | 978-1-7281-9697-8/21/$31.00 ©2021 IEEE | DOI: 10.1109/CAMA49227.2021.9703656

***Abstract*— New integrated high-resolution Spintronics Probe-Array at nanometric and micronic scales are proposed for very-near field (VNF) scanning and OTA-testing of electronic circuits and radiating systems. The proposed technology solutions lead to small dimensions (*micrometric range*), reduced cost, and high magnetic field sensitivity at room temperature with tunability through *smart-adaptive-biasing* control. The measured performances exhibit improvements in terms of accuracy and thermal stability outperforming state of the art sensors based on SQUID techniques, Josephson junctions or loops-based technologies. Porting of *chemically functionalized* Spintronics into advanced FD-SOI platforms is proposed as an enabler of hybrid *interferometric Thermal-Electromagnetic* sensing based on unified analog-digital *image-correlators* using ASIC-System on a Chip (ASIC-SoC) integration solutions.**

I. Introduction

Spintronic [1-2] devices exploit the spin of electrons to generate and control charge currents, and to inter-convert electrical and magnetic signals. Spintronics-based technology solutions enable the following possibilities [3-5]:

- *Co-integration* of sensor/antenna elements with Front-End-Modules (FEM) combined with smart digital-signal-processing (DSP) through a true Co-Design approach for pushing systems to their ultimate performances in advanced FDSOI [5-6] technologies.
- *Hybrid Interferometric EM-Thermal sensing* at nano-scale resolutions using *energy-based metrics* (Power-Density, Energy and Power Spectra, Entropy) for emerging new standards (e.g., SAR-based measurement in VNF) and applications (IoT & 5G/6G).

Furthermore, spintronic devices also cover a broad frequency spectrum from direct current (DC) to RF/mmWave, which could be useful for the on-chip generation and detection of high-frequency signals (FR2 bands and beyond). The ability to cast and implement Spintronic sensors in scalable arrays opens new avenues for real-time sensing and imaging of electromagnetic fields both for industrial and public applications [5]. Since the advent of early Near-Field Probe-Array technologies [7-9], progress in electronic technologies together with the development of modern signal processing techniques [10] have led to the proliferation of increasingly faster, accurate and cost effective Near-Field scanning systems. The rapidity of near-field probe-array solutions compared to conventional measurement techniques based on single probe mechanical scanning are now well recognized. However, among potential challenges for improving the performances of probe arrays are the sensitivity and dynamic range limitations, the interelement mutual coupling/interference, and the difficulties related to proper de-embedding of the probe array interaction with the Device Under Test.

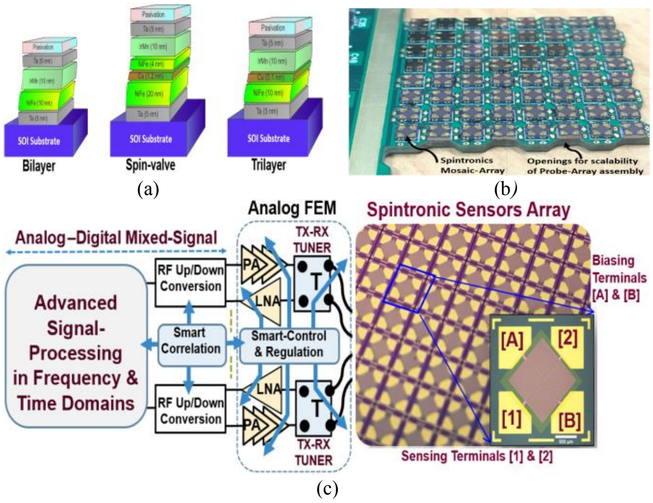

Fig.1: Spintronics technology stacks (a). Spintronics probe-array using 8x8 channels near-field scanner (b). Porting of spintronic sensors into FDSOI technology platform for unified co-integration with FEMs and DSP (c). Proposed canonical spintronic unitary cells are built as *4-terminal* devices.

In prior publication [1], we have presented the use of high-sensitivity Spintronic sensors for near-field magnetic-sensing of electronic circuits and radiating systems. Recently we have demonstrated hybrid magnetic and thermal near-field sensing with high resolution micronic spatial resolution for accurate extraction of correlated vital-signs [5]. The non-toxic quality of the chemically synthesized quantum spintronics material demonstrated in [5], combined with its low production cost, designates it as an excellent candidate for next generation smart IoT devices for medical applications. Beyond the medical applications, the proposed technology solutions enable new possibilities for VNF testing of circuits and OTA assessment of radiating systems.

In this contribution, we will present the practical use of industrialized spintronics-based sensors for very near-field measurement of electronic circuits and radiating systems. Spintronics sensors are very suitable for array applications due to their relatively small size and low power requirements when compared to coils or fluxgates and low-field sensing techniques, such as SQUIDs. Spintronic sensors lead to two orders of magnitude less power and at least three orders of magnitude lower cost than the competing technologies. In addition, since low magnetostriction alloys are used in the free sensing layers, incorporation on flexible substrates is also possible, enabling therefore conformal realization of OTA testing solutions. Unified co-integration of analog FEMs (*active circuitry such as LNAs, PAs, Switches, ADCs, etc...*) with Spintronics including advanced DSP is proposed through the porting of Spintronics hybrid Thermal-Electromagnetic sensing into advanced Fully Depleted Silicon-On-Insulator (FD-SOI) platforms [5-6] using ASIC-based System on a Chip (ASIC-SoC) technology solution.

II. Main Results, Analysis and Discussion

Spintronic devices by enabling new capabilities in the field of electromagnetic sensing bring challenges in link with materials, processes and circuits co-design and co-integration. In this section we focus on the following key enablers: the use of *high-sensitivity spintronics-based magnetic sensors* and the *functionalization of spintronics indicator material for imaging electromagnetic fields* through their *thermal signatures* using both IR and Visible imagers. We also discuss the challenges—at both the device and the system level—that need be addressed in order to co-integrate spintronic materials with Front-End-Modules combined with digital/analog signal processing and functionalities into OTA-testing for very-near field (VNF) scanning of electronic circuits and radiating systems.

Beyond OTA-based applications, the design and synthesis of functionalized molecules with controllable properties will foster new paradigms. These new paradigms will enable multifunctional materials hybridizing luminescence and chirality in order to drive the design of new optoelectronic devices with sensitivities and noise performances pushed to ultimate thermodynamic limits.

A. *High Sensitivity Spintronics-based Magnetic Sensors:*

The ability of the proposed spintronics magnetic sensors to operate at DC and at high frequencies make them excellent candidates for unified IoT and RF/mmWave solutions.

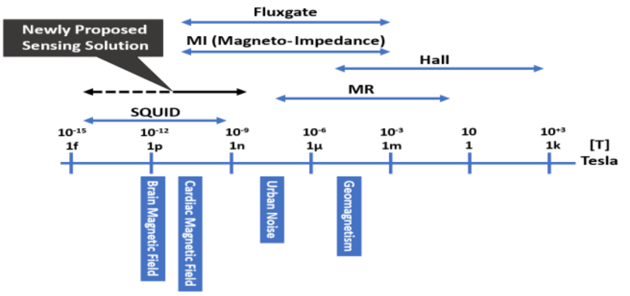

Fig.2: Positioning of the sensitivity of the proposed spintronics-based magnetic sensors compared to state of the art magnetic sensors.

The proposed IoT technological solution has been validated on an industrial scale for sensitivities in the *Nano-Tesla* range. Feasibility studies in progress show sensitivities in the *Pico-Tesla* range with the prospect of performances reaching the *Femto-Tesla* range which is currently only accessible through SQUID technologies (Fig.2). Sensitivity at *Femto-Tesla* range is required in order to deal with brain induced magnetic field levels while sensitivity in the *Pico-Tesla* range will be sufficient to detect magnetic fields radiated by human heart [11]. The challenge of reaching such low magnetic fields is not only a question of sensitivity but also a requirement of low-noise levels.

In this section, we conduct comparative analysis between the performances of the proposed spintronics-based high sensitivity magnetic sensors in Fig.3(a) and conventional coils in Fig.3(b) classically used in near-field-communication systems. Fig.3(c) represents a probe-array integrating 8×8 spintronics-based sensors with the signal processing and conditioning unit. The experimental setups in Fig.3(d) and Fig.3(e) are used for the calibration of the sensors using power-dependent stimuli as a function of frequency and operating conditions (*external fields, temperature, etc.*).

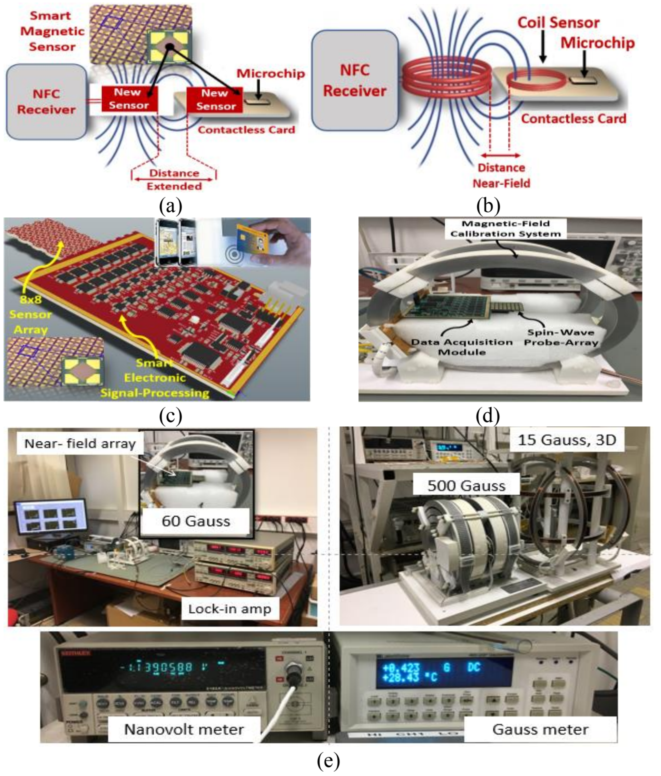

Fig.3: Proposed new spintronics-based (a) magnetic sensor for NFC. Classical coil-based (b) NFC systems. 8×8 probe-array realization using spintronics sensors combined with signal processing and conditioning module (c). In-house calibration setup for spintronics-based Probe-Arrays (d) accounting for power-levels and external fields stimuli (e).

A conventional magneto-inductive (MI) near field communication (NFC) system on the basis of a transmitter coil and a receiver coil has an effective distance $d_{T\text{-}R}$ proportional to the MI budget link as:

$$d_{T-R} = \sqrt[6]{\frac{P_T Q_T Q_R \eta_T \eta_R \mu_{r,T} \mu_{r,R} r_T^3 r_R^3 \pi^2}{P_R}} \tag{1}$$

where, P, Q, η, μ_r, r are corresponding to power, quality factor, coil coefficient, relative permeability of the core material of the coil and radius of the coil. T and R denote the transmitter and the receiver.

With dedicated transmitter and receiver coils, the distance reduces quickly proportional to 6^{th} root of the transmit power (P_T). Therefore, the effective communication distance is limited in this *coil-to-coil* communication technique.

Following the advancement of spintronic sensors in the detection of nanotesla range of magnetic field and beyond, a new communication solution on the basis of a transmitter coil and a spintronic sensor configuration results in significant improvement of the effective detection range. In this communication configuration, the detection distance between sensor coil and spintronic sensor, $d_{c\text{-}s}$, can be evaluated by Biot-Savart law. When $d_{c\text{-}s}$ is much greater than the radius of the transmitter coil, the effective communication distance can be deduced using the following expression:

$$d_{c-s} = \left(\frac{\mu_0 \mu_{r,c} N I r_c^2}{2B}\right)^{\frac{1}{3}} \tag{2}$$

Here μ_0, $\mu_{r,c}$ are magnetic permeability of air, and relative permeability of the core materials of the transmitter coil.

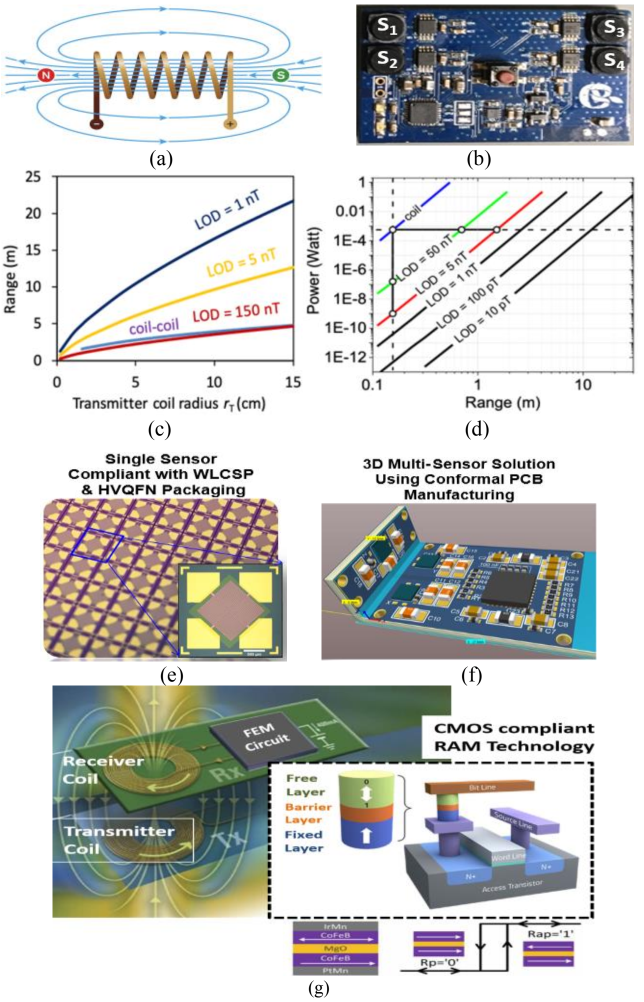

Fig. 4: Comparative measurement of a coil-to-coil communication and coil-to-sensor communication systems. (a) a transmitter coil excites an electromagnetic field detected by our spintronic sensor board (b). (c) detection range of the coil-coil communication and coil-sensor communication methods versus the radius of the transmitter coil. (d) Required emitting power versus detection range of a receiver coil and spintronic sensor at different detection threshold levels. Replacement of classical coil-based magnetic sensors by CMOS-compliant (e.g., FDSOI) RAM [12-13] building blocks for On-Chip co-integration of FEMs with spintronic sensors (e) in 3D WLCSP integration (f),(g).

N, r_c and I, are the number of turns, radius of the transmitter coil and the electrical current through the transmitter coil, respectively. B is the threshold in detection of magnetic field of the spintronic sensor. The detectable ranges of the coil-to-coil and the coil-to-sensor, for NFC communications, as a function of transmitter coil radius are calculated using equations (1) and (2). In the coil-to-coil configuration, the receiver coil is made of 20 turns and a radius of 15 mm, the transmitter coil having 70 turns and variable radius. In the coil-to-sensor configuration, the transmitter coil is the same as in the coil-to-coil NFC system, the spintronic sensor having an equivalent noise of $10\,pT/\sqrt{Hz}$ in a wide frequency band. In Fig.4(b), we present the NFC board integrating spintronic sensors, FEMs, ADCs and signal processing unit. In Fig.4(c), effective distance of the coil-to-coil NFC system is compared to the configuration of coil-to-sensor based solution setup at different limits of detection (LOD) standing for B in equation (2). The results evidenced that the effective range of coil-to-coil NFC system is comparable to the coil-to-sensor NFC system in the case of spintronic sensor having 150 nT resolution.

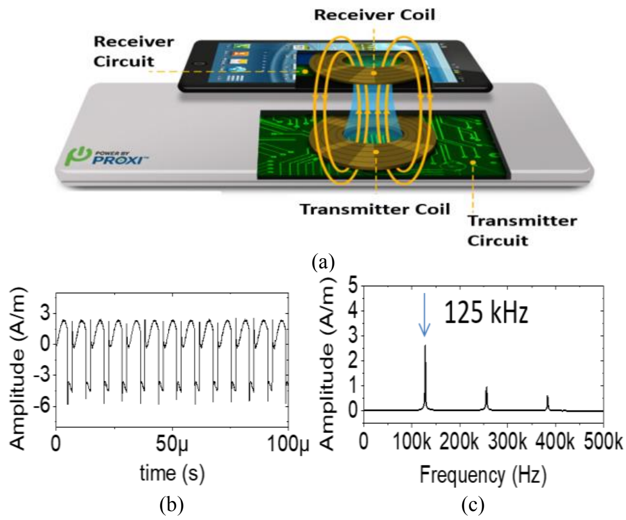

Fig. 5: (a) Schematic of a wireless charging system. (b), (c) electromagnetic field in time and frequency domains measured by a spintronic sensor at the wireless power transfer zone of a commercial smartphone charger (*Apple MagSafe* charger).

Obviously, with low field resolution of our spintronic sensor, the coil-to-sensor NFC system will result in great advantages over the actual NFC system. For example, in Fig. 4(d), we plotted the required power biasing for the transmitter coil versus effective range for the coil-to-coil and the coil-to-sensor NFC system. We can deduce from these measurements clear statement: with the same biasing power of the transmitter coil, much greater effective distance is achieved with low resolution spintronic sensor (*10 m for sensor of 10 pT resolution*) compared to the receiver coil, (*20 cm for coil of 20 turns with a radius of 15 mm*). In another context, to obtain the same effective distance, the required biasing power for the transmitter is much lower for the case using spintronic sensor (*in the range of femtoWatt*). In order to obtain similar performances using a receiver coil as detector, power levels at least in the range of milliwatts are required. Such performances can be beneficial for emerging wireless power-transfer systems widely deployed in many mobile devices. For high end-to-end power transfer efficiency, design of charging system is based on the induction concept (Fig. 5(a)). A DC voltage at the base station is converted into an AC current through a transmitter coil at a frequency in the range from few tens to few hundreds of kilohertz. AC current in the coil radiates an electromagnetic field. The electromagnetic field will induce an AC current in a receiver coil when the load device is in close proximity. Due to the inverse square law, the field strength generated by the transmitter coil reduces rapidly with vertical distance. Therefore, to optimize the efficiency of power transfer, the receiver coil should have optimal dimensions, parallel alignment and small vertical distance to the transmitter coil. To align the two coils, magnetic alignment method using a permanent magnet (*e.g., Apple MagSafe charger*) is introduced. With high sensitivity in measurement of magnetic field from DC to high frequency, our spintronics sensor can be used to measure *both* the AC and DC magnetic field generated from *Apple MagSafe* charger in time and frequency domains as shown in Fig. 5(b) and 5(c). In another use case, a levitating bulb system, the bulb being levitated by a magnetic force, and the power to light up the bulb is transferred to light up the bulb wirelessly from the based station (Fig. 6(a)). To levitate and balance the bulb, a permanent magnet in the shape of a ring and electromagnetic coils system are employed. To levitate the bulb stably, the electromagnetic coils system is regulated to compensate the imbalance resulting from field variations of the permanent magnet ring by an adaptive real-time voltage control. In this system, the AC field comprises two components emitted from the regulating electromagnet coils and from the power transfer coil. The frequencies of regulated field and power transfer field are different to avoid interferences.

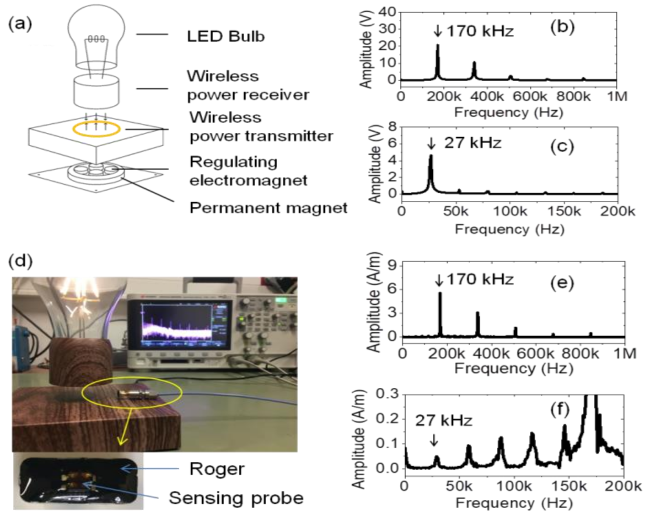

Fig. 6: Levitating bulb with real-time regulation and wireless power transfer measurements validation. (a) Schematic of a levitating bulb system; (b-c) voltage excitation at the regulating magnet for balancing the bulb and voltage at the transmitter coil for power transfer; (d) image of the measurement setup using a spintronic sensor to probe the EM field radiated from the levitating bulb system; (d-f) radiated magnetic fields measured by a spintronic probe.

Biasing voltage for the regulating electromagnetic coils and power transfer coil are measured and shown in Fig. 6(b) and Fig.6(c). We observe a stable voltage of 22 *Vp* at 170 kHz biasing the power transfer coil, another voltage biasing the electromagnet system at a frequency of 27 kHz with varying amplitude from 0 to 5 *Vp*. To measure the electromagnetic field created by these two coils, a spintronic sensor connected through Rogers material for low loss detection of AC magnetic field (Fig. 6(d)) in the band DC-40GHz is used. The measured amplitudes of electromagnetic field in two frequency ranges of 0 - 1 MHz and 0 - 200 kHz are plotted in Fig.6(e) and Fig.6(f) to highlight the magnetic fields generated by the transmitter coil and regulating electromagnetic coils at the two reference frequencies of 170 kHz and 27 kHz, respectively. The results reveal the merit of our spintronics sensor in measuring magnetic fields in two frequency bands of a levitating bulb Device Under Test (DUT) in a non destructive way, simultaneously. One of the major advantages of our spintronic sensor compared to an electromagnetic sensing loop is its ultrahigh sensitivity in detection of DC and AC magnetic fields with low biasing power. This enables the realization of large scale and highly dense arrays with low power consumption. Fig.7(a) shows the schematic of array 16 × 16 sensors and the image of its integrated circuit. The whole sensing array requires a power consumption of 130 milliwatts. The sensor array is arranged for the detection of magnetic fields in x-axis and y-axis simultaneously. The used photolithography at chip level enables sensor array resolutions below micronic scales. Unitary sensor cells can be designed to natively encompass 3 component detections.

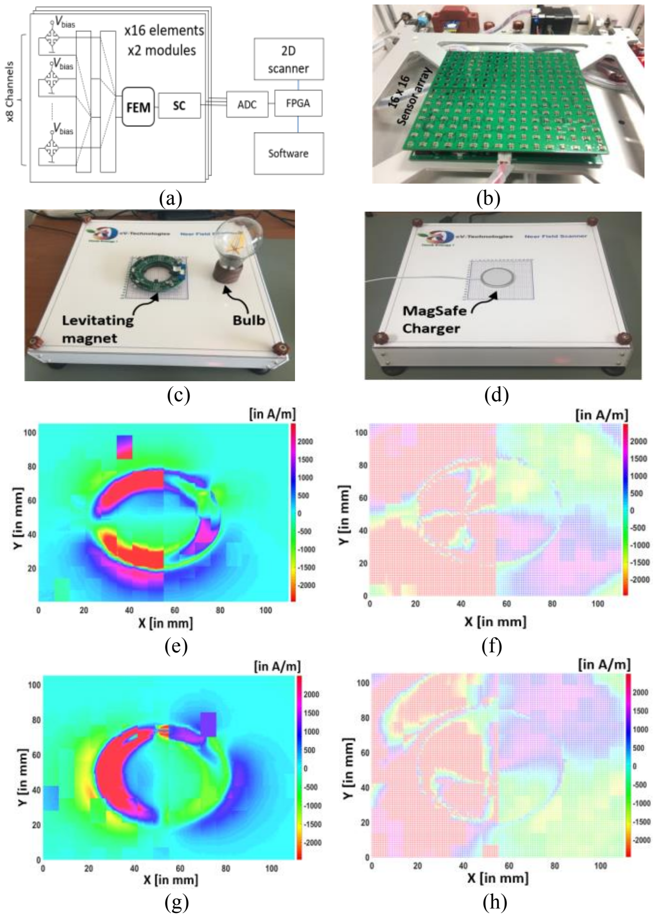

Fig.7: Spintronics near-field scanner probe-array. a) synoptic view of the 16×16 probe-array. b) image of the embedded sensor array on the 2D scanner module; c) image of the NFS system with a levitating bulb DUT and the measured DC field distribution in X-axis and Y-axis at a distance of 15 mm on top of the ring magnet; d) image of the NFS system with a MagSafe charger as DUT and the scanning result of DC magnetic field distribution on top of the charger at a distance of 30 mm. Measured near-field scans of X (e) and Y(g) components of the magnetic field for the levitation system DUT. Measured near-field scans of X (f) and Y(h) components of the charger.

The array is mounted on a 2D scanner stage with a programmable scanning pitch from 7.5 mm down to 50 µm to map the magnetic field of the DUT in real-time or in high spatial resolution. The magnetic field scale of the array can be controlled from 15 kA/m down to 40 A/m or lower. Fig.7(c) and 7(d) respectively present use-cases for the levitating bulb and the smartphone charger (*MagSafe*). The 3D heat maps in x and y axis of the magnetic field are the results of high spatial resolution scanning at 50 µm pitch. The NFS system allows mapping of magnetic field at different vertical heights with configurable high precision and low spatial resolutions. The used spintronic magnetic sensors can be hybridized with spin crossover functionalized materials toward Thermal-Electromagnetic interferometric sensing.

B. *Spintronics-based EM-Thermal Co-Design Toward High-Resolution Near-Field Sensing of Power and Energy Density Metrics*

Use of electromagnetic infrared techniques for visualizing and measuring microwave fields is well known [14-17], following the pioneering work of Hasegawa [18] in 1995. The available techniques consist in inserting sensitive films with electric and/or magnetic properties which induce currents resulting in heating recorded by the infrared cameras. However, today, to our best knowledge available solutions are based on materials that demand for high input powers up to several tens of dBm which lead to low heating effects very difficult to use for OTA-Testing of devices and systems. We propose alternative solutions based on the use of quantum spin-crossover (SCO) materials [3] exhibiting functional properties which are responsive to multi-physics external stimuli such as temperature, pressure, light irradiation, electromagnetic field, radiation, nuclear decay, soft-X-ray, (de)solvation. We introduce new Electromagnetic-Thermal sensing [5] solutions using SCO materials for near-field and far-field characterization of electronic circuits and radiating systems. Use of innovative correlation technologies [19] is combined with advanced interferometric synchronized sampling for accurate extraction of vectorial power and energy density metrics in time and frequency domains.

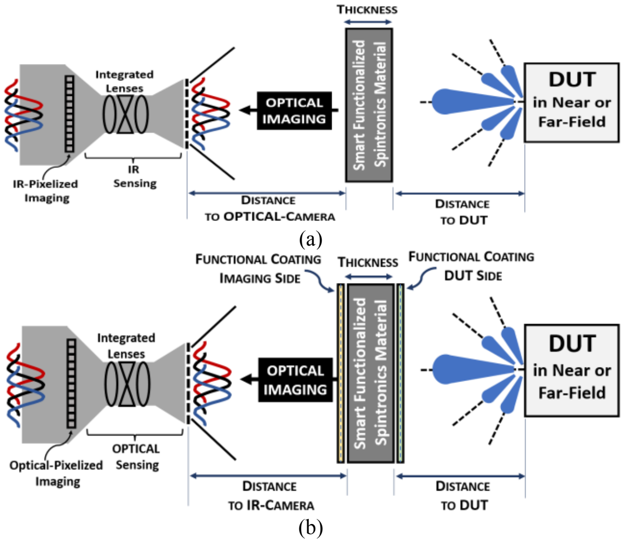

Fig. 8: Smart functionalized spintronics material for Electromagnetic-Thermal sensing in near and far field using IR-Camera (a). Functionalized spintronics material with coating for Electromagnetic-Thermal sensing in near and far field using Optical-Camera (b).

Fig.8 illustrates the synoptic view of the proposed Electromagnetic-Thermal conversions using both IR-cameras in Fig.8(a) and visible cameras in Fig.8(b). In Fig.8(b), two separate functionalizations are considered distinctly for the coating of the SCO material on the DUT side and on the IR/Visible camera side. The proposed EM-Thermal sensing solutions are evaluated using 5G NR FR2 antenna array (1×4 elements) module as DUT for frequencies in the band from 26 GHz to 30 GHz. The unitary antenna element composing the array is based on the aperture-coupled structure introduced in [20]. A 4×4 mm² patch is placed at 2 mm above the upper slot introducing an additional resonance which allows the single-element bandwidth and gain to be increased. The antenna module is connectorized (see Fig.9(a)-(d)) for a 4-Port measurement configuration using both frequency and time-domain instruments with and without down-conversion to sub-6 GHz frequency bands. Using distributed power-combining structures, the 4-Port antenna module can be excited using adjustable amplitude and phase values for beamforming in Fig.9(e)-(f). In Fig.9(e)-(f), the Electromagnetic-Thermal sensing reference plane for power and energy density is at 10 mm above the DUT, which is the bottom of the thermal indictor material. The thickness of the indicator material is varied from few tens of microns to few hundreds of microns. Specific attention is directed toward proper shielding of unwanted convection effects.

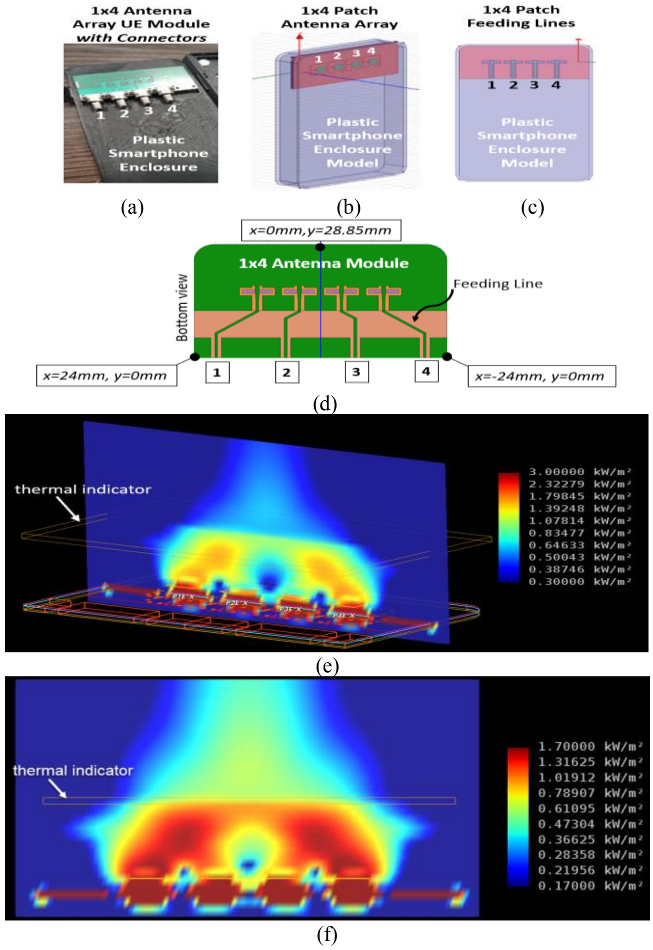

Fig. 9: Experimental 26 GHz DUT with connectorized 1x4 antenna array in User-Equipment (a) and associated 3D Model including enclosure (b) and feeding lines (c) built using Full-Wave solvers in time and frequency domains. DUT near-field scanning area for power & energy density extractions (d). Energy-Density at 26 GHz in 3D (e) and xz (f) side views for simultaneous excitations with 0° phase difference at 23dBm input power.

It is observed that a direct link can be established between the thermal variations on the indicator material and the square of the electric (or magnetic) field. Few tens of dBm input power feeding the radiating elements will lead to few degrees heating dynamic on the used thermal indicator from which field amplitudes can be deduced following simple relations:

- *For Electric-Field as primary sensing field:*

$$|E| = \mathrm{X}^{\mathrm{E}}_{\mathrm{EM-Thermal}}\sqrt{\Delta T_{Averaged}} \quad (3)$$

- *For Magnetic-Field as primary sensing field:*

$$|H| = \mathrm{X}^{\mathrm{H}}_{\mathrm{EM-Thermal}}\sqrt{\Delta T_{Averaged}} \quad (4)$$

In equations (3) and (4) $\mathrm{X}^{\mathrm{E}}_{\mathrm{EM-Thermal}}$ and $\mathrm{X}^{\mathrm{H}}_{\mathrm{EM-Thermal}}$ are conversion coefficients that depend on the heat transfer coefficient, the heat capacity, the density of the thermal indicator material, and the frequency. From equations (3) and (4) the power density (spatially averaged) appears in the form:

$$|sPD| = \propto \mathrm{X}^{E}_{EM-Thermal}\mathrm{X}^{H}_{EM-Thermal}\Delta T_{Averaged} \quad (5)$$

In Fig.10(e) and Fig.10(f) a setup based on the configuration of Fig.8(a) is used in reference to a thermal indicator material with tan(δ)=0.022. The thermal conductivity of the thermal indicator material is 0.2 W/(m.K) for a convection coefficient of 15.3 W/(m^2.K) and a relative radiation coefficient equal to 1. The EM-Thermal co-design model is meshed using 5.3 Mcells (334×52×104).

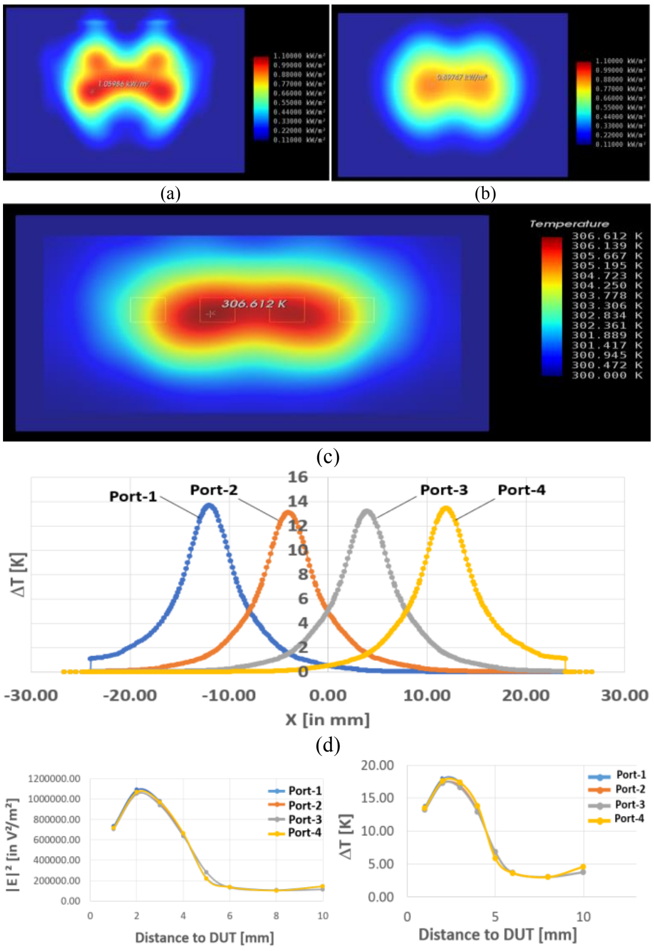

(a) (b) (c) (d) (e) (f)

Fig.10: Extracted power density (a) and averaged power-density (b) for excitation 0° phase offset. Extracted thermal distribution (c) on the thermal indicator material. Extracted thermal distribution for sequential excitations of the four ports of the DUT (d). Square of E-Field magnitude (e) and temperature variation (f) on the thermal indicator material as a function of separation distance between the DUT and the thermal indicator material.

Fig.10(a) and Fig.10(b) represents the power-density and averaged power-density for simultaneous excitations with 0° phase offset. In Fig.10(c) the temperature distribution on the indicator material is presented. Fig.10(d) depicts extracted temperature variations as function of sequential antenna elements excitations. Fig.10(e) and Fig.10(f), respectively, show the square of the magnitude of the electric field and the temperature variation on the thermal indicator material as a function of separation distance from the DUT.

III. Conclusion

In this paper, new integrated high-resolution Spintronic Probe-Array at nanometric and micronic scales are proposed for very-near field (VNF) scanning and OTA-testing of electronic circuits and radiating systems with detected fields ranging from few tens *mT* down to tens *pT*, therefore spanning about 10 orders of magnitude in the magnetic field range. The measured performances exhibit improvements in terms of accuracy and thermal stability outperforming state of the art sensors based on SQUID techniques, Josephson junctions or loops-based technologies. Innovative near-field and far-field imaging of electromagnetic fields through their thermal signatures on an indicator quantum spin-crossover (SCO) material using both IR and Visible imagers is presented. The Thermal-EM imaging solution has been applied to RF/mmWave beamforming modules demonstrating the possibility of extracting *power-density* and *energy-density* metrics *as function of beamforming angles*. Porting of Spintronics sensing solutions into advanced FD-SOI platforms will facilitate the unification of IoT and RF/mmWave technologies. The co-integration of *functionalized spintronic materials* with smart FEMs will foster new possibilities for cognitive Thermal-EM imaging.

Acknowledgment

The authors thank Prof. Jean-Charles Bolomey for fruitful discussions during the preparation of the paper. The authors are grateful to Dr. Volker Muehlhaus and Dr. David Schäfer for collaborations on Electromagnetic-Thermal co-analysis using IMST-EMPIRE 3D solutions. The authors thank Prof. Fabien Ferrero and the joint CREMANT/ORANGE Lab for collaboration on RF/mmWave Power-Density measurements.

References

[1] Q.H. Tran, S. Wane, et al., “Toward Co-Design of Spin-Wave Sensors with RFIC Building Blocks for Emerging Technologies", 2018 2nd URSI Atlantic Radio Science Meeting (AT-RASC)”.

[2] P. P. Freitas, et al., “Spintronic Sensors” Proc. of the IEEE 104 (10)1894 (2016)DOI: 10.1109/JPROC.2016.2578303.

[3] G. Molnár, et al., “Molecular spin crossover materials: Review of the lattice dynamical properties”, Ann. Phys., 531(10), 1900076, 2019.

[4] Kraieva, C.M. Quintero, et al., “High spatial resolution imaging of transient thermal events using materials with thermal memory” Small 12 (2016) 6325–63314.

[5] S. Wane, Q.H. Tran, et al., “Smart Sensing of Vital-Signs: Co-Design of Tunable Quantum-Spin Crossover Materials with Secure Photonics and RF Front-End-Module”, IEEE-MTT-Texas symposium 2021.

[6] Bich-Yen Nguyen, et al., “A Path to Energy Efficiency and Reliability for ICs: Fully Depleted Silicon-on-Insulator (FD-SOI) Devices Offer Many Advantages”, IEEE Solid-State Circuits Mag. (Volume: 10, Issue: 4 , Fall 2018).

[7] Bolomey, J.C., et al., "Rapid Near-Field Antenna Testing via Arrays of Modulated Scattering Probes," IEEE Trans. on Ant. and Prop., vol. 36, no. 6, pp. 804-814, June 1988.

[8] Bolomey, J.C. and F.E. Gardiol, Engineering Applications of the Modulated Scatterer Technique, Artech House, Norwood, MA, 2001.

[9] B.Fourestie, J.-C. Bolomey, et al., “Spherical Near Field Facility for Characterizing Random Emissions”, IEEE Trans. On Ant. and Prop., Vol. 53, no. 8, pp. 2582-2588, August 2005.

[10] M.Sierra-Castaner, L.J.Foged, Post-Processing Techniques in Antenna Measurement. The Institution of Engineering and Technology: London, UK, 2019.

[11] G. M. Baule and R. McFee, “Detection of the magnetic field of the heart,” Am. Heart J. 66, 95–96 (1963).

[12] L. V. Cargnini, et al., “Embedded Memory Hierarchy Exploration Based on Magnetic Random Access Memory”. Journal of Low Power Electronics and Applications, MDPI, 2014, 4 (3), pp.214-230.

[13] L. Nyssens et al., “28 FDSOI RF figures of merit down to 4.2 K,” in Proc. IEEE SOI-3D-Subthreshold Microelectron. Technol. Unified Conf. (S3S), San Jose, CA, USA, 2019.

[14] P. Levesque and L. Leylekian, “Capteur vectoriel de champs électromagnétique par thermographie infrarouge,” French Patent 9 816 079, Dec. 17, 1998.

[15] D. Prost, F. Issac, F. Lemaitre, J.P. Parmantier “Infrared Thermography of Microwave Electromagnetic Fields”, D, EMC Europe, Rome, (2012).

[16] H. Ragazzo, et al., “Detection and imaging of magnetic field in the microwave regime with a combination of magnetic losses material and thermofluorescent molecules,” IEEE Trans. Magn., vol. 55, no. 2, pp. 1–4, Feb. 2019, doi: 10.1109/TMAG.2018.2860520.

[17] C. Baer, K. Orend, B. Hattenhorst, T. Much, “Field Representation Microwave Thermography Utilizing Lossy Microwave Design Materials”. Sensors 21(14): 4830 (2021).

[18] T. Hasegawa, “A new method of observing electromagnetic fields at high frequencies by use of test paper", Bull. Yamagata Univ. IV, Japan, 1995.

[19] S. Wane, et al., “Correlation Technologies for OTA Testing of Mobile Devices: Power-Density Measurement”, in IEEE Conf. on Ant. Measurements Applications, Nov. 2021.

[20] T.Q.K. Nguyen, et al., “Experimental evaluation of user's finger effects on a 5G terminal antenna array at 26 GHz”. IEEE Antennas Wirel. Propag. Lett., 1–1 (2020).